APPLIED PHYSICS LETTERS 104, 021604 (2014)

Correlation between the electronic and atomic structure, transport properties, and oxygen vacancies on $La_{0.7}Ca_{0.3}MnO_3$ thin films

J. Rubio-Zuazo,[1,2,a)] L. Onandia,[1,2,b)] P. Ferrer,[3] and G. R. Castro[1,2]
[1]*Spanish CRG BM25-SpLine beamline at the ESRF, 6 Rue Jules Horowitz, BP 220, F-38043 Grenoble Cedex 09, France*
[2]*Instituto de Ciencia de Materiales de Madrid—ICMM/CSIC, Cantoblanco, E-28049 Madrid, Spain*
[3]*Diamond Light Source, Harwell Science and Innovation Campus, Chilton, Didcot OX11 0DE, United Kingdom*

(Received 21 October 2013; accepted 20 December 2013; published online 16 January 2014)

We present a study of the role of oxygen vacancies on the atomic and electronic structure and transport properties on a 20 nm thick $La_{0.7}Ca_{0.3}MnO_3$ film grown by the pulsed laser deposition method on a $SrTiO_3$ (001) substrate. The results show that oxygen vacancies induce an atomic structure modification characterized by the movement of the La/Ca cations to the perovskite regular position, by the reduction of the MnO_6 basal plane rotation, and by a cooperative tilting of the octahedra along the out-of-plane direction. The out-of-plane lattice parameter increases due to the reduction of the Mn valence upon oxygen vacancies creation. As a consequence, a shift of the Metal-to-Insulator transition to lower temperatures is found to occur. We discuss the influence of the competitive phenomena of manganese valence and Mn-O-Mn bond distortion on the transport properties of manganite thin films. © *2014 AIP Publishing LLC*.
[http://dx.doi.org/10.1063/1.4861385]

Complex oxides have been widely studied since many years because they show exotic behaviors as superconductivity, colossal magnetoresistance, charge ordering, ferroelectricity, or multiferroicity. In most of the cases, such phenomena are a consequence of an intricate interplay of charge, spin, orbital, and lattice degrees of freedom. The growth of these materials in thin film form usually modifies its intrinsic properties hampering their potential application in industrial devices. This is the case of La-Ca mixed-valence manganites. Even the most stable manganites (1/3 doping) show a strong degradation of its magneto-electric properties when growth in thin film form with respect to bulk compounds. A decrease of the Curie (Tc) and metal-to-insulator (MIT) transition temperatures occur as the thin film thickness is reduced.[1–3] Such a behavior seems to be an unavoidable property of heterostructures with half-metallic oxides. Several models as the existence of an electrical dead layer,[3] a bandwidth modification due to the Mn-O-Mn bond angle distortion[4] or multiple phase segregation,[5] joined to a crystal structure modification depending on the chosen substrate[6,7] have been used to explain the anomalous behaviour of ultra-thin films compared to bulk. Other models as phase separation[8] or electron (spin) confinement[1] are also used to explain the observed properties. Unless less studied, the oxygen vacancies induce strong lattice distortions due to important changes in the cation stoichiometry, which influences the thin film transport properties. Based on the Double Exchange (DE) model, the itinerant eg electron promotes from the Mn^{3+} to the Mn^{4+} ions through the oxygen cation. The Mn-O-Mn bond angle and bond length, i.e., crystal atomic structure, which are strongly dependent on oxygen vacancies, drives the transport properties and the magnetoresistance behavior. The detailed determination of the structural, electronic and transport properties of manganites thin films induced by the oxygen vacancies is crucial for optimizing the films quality, and hence for increasing the efficiency of electronic complex-oxides based devices. Despite the long history of work on this material, there has been no systematic investigation on the role of the oxygen vacancies on the evolution of the mechanisms occurring in the film. In this letter, we present the correlation between the atomic structure, electronic and transport properties with the oxygen vacancies on a 20 nm thick $La_{0.7}Ca_{0.3}MnO_{3-\delta}$ ($0 < \delta < 0.21$) film. We discuss the influence of the competitive phenomena of manganese valence and Mn-O-Mn bond distortion on the transport properties of manganite thin films.

A 20 nm thickness layer of $La_{0.7}Ca_{0.3}MnO_3$ (LCMO) was grown on $SrTiO_3$ (001) (STO) substrate by the pulsed laser deposition method using a Nd:YAG laser with 355 nm wavelength, 10 Hz, and 1 J/cm^2 irradiance power. A stoichiometric polycrystalline $La_{0.7}Ca_{0.3}MnO_3$ target was used. The thin film was deposited in an oxygen atmosphere of 2 mbars keeping the substrate at room temperature. After growth, the sample was annealed at 1000 K in 1 bar of flowing oxygen during 40 min. The thickness of the film was obtained by low angle X-ray diffraction. After sample insertion on the analysis chamber, oxygen vacancies are created by sample heating under ultra-high vacuum conditions. The atomic and electronic structure and oxygen content are followed simultaneously by X-ray diffraction (XRD) and Hard X-Ray photoelectron spectroscopy (HAXPES) at the BM25-SpLine beamline (Branch B) at the ESRF. Photon energy of 12 keV was used ensuring accessibility to a wide reciprocal space region and creating electrons with high enough kinetic energy to probe the whole layer. *Ex-situ* transport

[a)]Author to whom correspondence should be addressed. Tel.: +33 476881782. Fax: +33 476882816. Electronic mail: rubio@esrf.fr
[b)]Author Information Note: Laura Onandia was dead in Grenoble-France on 26th March 2013.

measurements in the film plane were performed by the conventional two probe method at different levels of sample de-oxygenation. As soon as the transport measurements were finished, the sample was introduced inside the analysis chamber to continue the de-oxygenation process. During the whole de-oxygenation process, the vacuum in the analysis chamber was in the 10^{-10} Torr range. Turbo-molecular, ionic, Ti-sublimation, and getter pumps were used to pump the oxygen released by the sample so to maintain the ultra-high vacuum (UHV) conditions.

The LCMO ideal bulk structure is an orthorhombic distorted perovskite described by the $D_{2h}^{16} - Pbnm$ symmetry space group.[9] The distortion caused by the cation size mismatch is alleviated by a cooperative rotation of the MnO_6 octahedron about the [001] axis and a tilt about the [110] axis. Hence, the chain of octahedrons forms a zig-zag structure along the [001] direction. The La^{3+} and Ca^{2+} shift from their ideal position according to the octahedron displacements. Therefore, the divalent and trivalent cations will follow the MnO_6 octahedron zig-zag structure along the [001] direction. Due to the zig-zag type structure, the unit cell doubles its dimension along the out-of-plane axis (a_3-axis) respect to the cubic perovskite structure. The unit cell is then composed of 20 atoms arranged according to the symmetry conditions.[9] In the case of epitaxial thin films, the in plane lattice parameter a_1 and a_2 matches those of the substrate. As the LCMO in-plane lattice parameter is $a_1 \cong a_2 \cong \sqrt{2}a_{STO}$, the manganite grows with its crystallographic axis along the (11) and (1-1) direction of the STO substrate, i.e., both lattices are rotated by 45°, in order to minimize the lattice mismatch (1%) between both materials. The LCMO out-of-plane lattice parameter is $a_3 \leq 2a_{STO}$. The miller indices of the orthorhombic space group are then $(h+k, h-k, 2l)$, where h, k, and l are the indices of the cubic STO. It is expected that the STO only contributes to the diffraction signal for the reflections with integer h, k, and l values. However, due to the rotation angle present between both lattices and due to the double out-of-plane lattice parameter of the LCMO respect to the STO, it is expected that the manganite film presents extra peaks at half-integer h, k, and l values. Figures 1(a)–1(c) show l scans along the (1 0 l), (1.5 0.5 l), and (1.5 1.5 l) cubic directions for the sample as-grown (top curve), i.e., without oxygen deficiency, and with different levels of oxygen vacancies (increasing oxygen deficiency from top to bottom curves). The extinction conditions obtained from the diffraction patterns correspond to the bulk LCMO structure for the as-grown sample. It can be clearly seen that some of the diffracted peaks from the LCMO thin film changes its relative intensity as the thin film is heated in a vacuum atmosphere. Specifically, the half-integer l-peaks from the reflections with integer h and k values, and the integer l-peaks from the reflections with half-integer h and k values, diminish its intensity. The intensity of these peaks for the sample heated 2 (treatment a) and 10 min (treatment b) at 600 K under vacuum decreases 60% and 95%, respectively, respect to the as-grown sample. The sample was then maintained at 600 K for 1 h without appreciable modification of the diffraction pattern. The peaks are completely absent after further heating the sample 5 min at 675 K (treatment c).

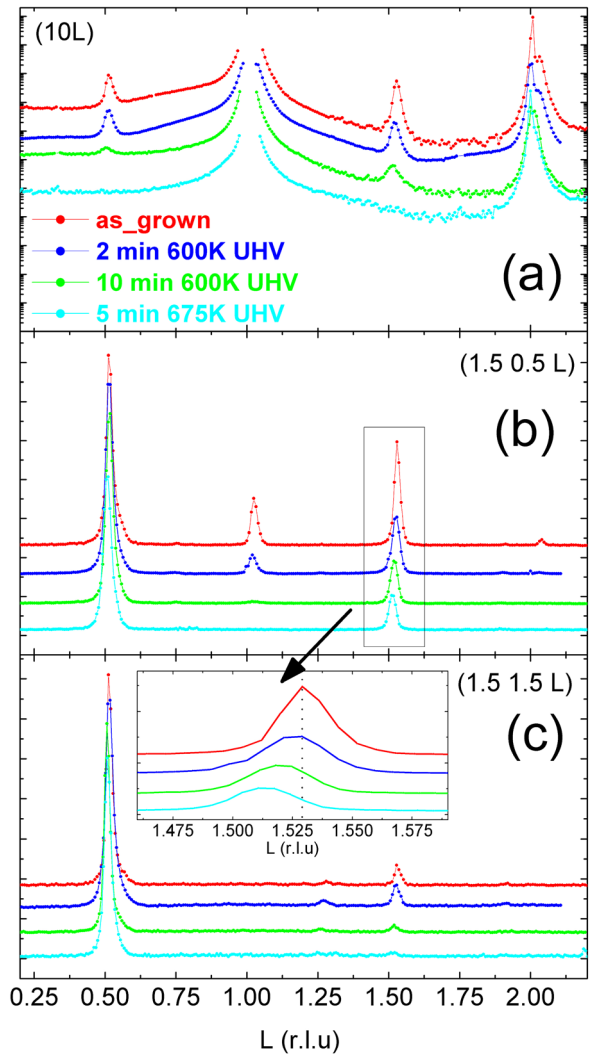

FIG. 1. XRD patterns along the out-of-plane directions (a) (1 0 l), (b) (1.5 0.5 l), and (c) (1.5 1.5 l) for the sample without oxygen vacancies (top curve) and for different levels of oxygen deficiency (increasing oxygen deficiency from top to bottom curves). h, k, l are referred to the $SrTiO_3$ cubic lattice. Inset: expanded region for the reflection (1.5 0.5 1.5).

We have evaluated the effects on the diffraction patterns of different atomic displacements from a tetragonal perovskite according to the symmetry conditions imposed by the *Pbnm* space group. The structure factor of the reflections with integer h and k and half-integer l values is mainly determined by the La-Ca ions displacements [Wyckoff 4c]. The octahedral basal plane rotation and tilt distortions [Wyckoff 8d] are the main responsible for the diffraction intensity for the reflections with half-integer h and k values and integer l-values. In summary, the oxygen vacancies induce a structural modification, where the La and Ca ions are displaced toward their regular position of the ideal perovskite and the MnO_6 block tends to be coplanar aligning the Mn-O-Mn bonding (180° angle). However, a cooperative displacement of the apical oxygen atoms remains present preserving the approximated double out-of-plane lattice parameter. For treatment c, the La and Ca ions retrieve the undistorted position of the regular perovskite and the octahedral basal plane remains coplanar with a Mn-O-Mn bonding angle of 180°. Also, the diffraction pattern reveals (Inset Figure 1(c)) an enlargement of the out-of-plane lattice parameter with

increasing the oxygen deficiency. Such an effect is the result of the increase of the average manganese ionic size increase induced by the oxygen vacancies.

Figure 2 shows the temperature dependent resistance curves for the different annealing treatments. All the samples showed a metal to insulator transition, but at different temperatures. The MIT for the as-grown sample is 265 K, which corresponds to the value reported for fully oxygenated and stoichiometric bulk $La_{0.7}Ca_{0.3}MnO_3$. The MIT is lowered with the increase of oxygen vacancies. We obtained a MIT of 170 K and 28 K for treatment a and b. The transition temperature shifts back to higher temperatures (MIT = 54 K) for treatment c. As shown above by XRD, at this stage of de-oxygenation, the obtained diffracted pattern is compatible with an atomic structure characterized by the perfect alignment of the Mn-O-Mn bond, with the consequent increase of the hopping of the itinerant electron. Such a fact gives direct evidence of the important role of the atomic structure on the double exchange model used to describe the fundamental properties of manganites.

Figure 3 shows the O 1s (a), La 3d (b), and Mn 3s (c) HAXPES spectra for the different sample treatments (increasing oxygen deficiency from top to bottom curves). It should be stressed that the electron kinetic energy for the probed core levels ranges between 11 keV and 12 keV for the photon energy used. The information depth of such high kinetic energy electrons is of the order of 50 nm,[10] being hence much larger than the thickness of the studied sample. In this way, the electronic properties and oxygen content obtained from the HAXPES spectra are related to the whole layer thickness and not only to the first monolayers. The analysis of the O 1s core level photoemission peak provides direct quantification of the average oxygen deficiency respect to the as-grown sample. From the photoemission intensity variation, we have obtained 2% ($\delta = 0.06$), 5% ($\delta = 0.15$), and 7% ($\delta = 0.21$) of oxygen vacancies for sample treatment a, b, and c, respectively. The La 3d HAXPES spectra show the expected doublet corresponding to the spin-orbit splitting accompanied by satellites of comparable intensity. The intensity and separation of these satellites respect to the main peak, which are assigned to electron transfer process,[11–13] provide a fingerprint to identify the La (III) oxide compound. We have obtained an energy separation of 17.1 eV ± 0.1 eV between the $3d_{3/2}$ and $3d_{5/2}$ photoemission peaks and 4.2 eV ± 0.1 eV for the satellites, corresponding to the La_2O_3 compound.[14]

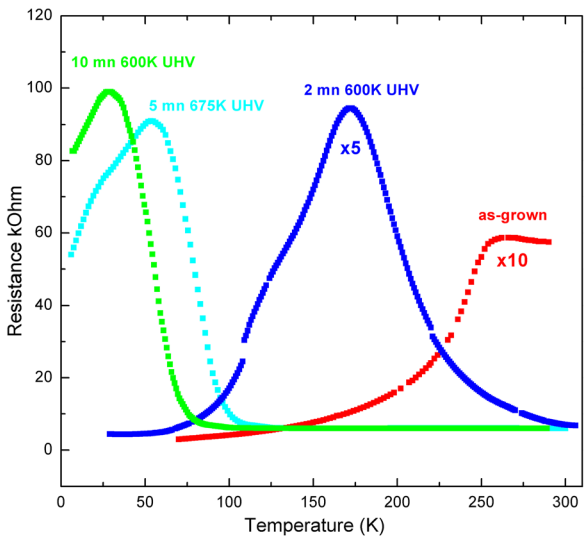

FIG. 2. Temperature dependent resistance curves for different annealing treatments. The metal-to-insulator transition shifts to lower temperatures as the oxygen deficiency is increased, except for the annealing at 675 K in UHV during 5 min for which the transition shifts back to higher temperatures.

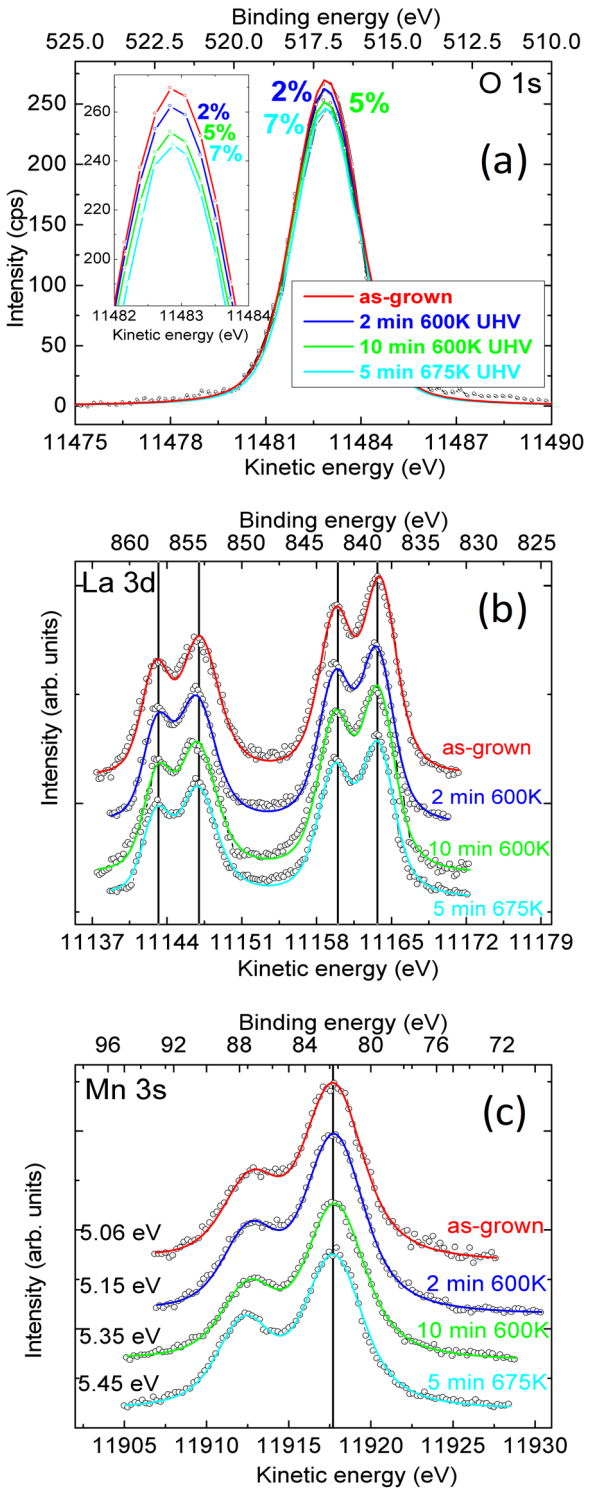

FIG. 3. (a) O 1s, (b) La 3d, and (c) Mn 3s, Hard X-ray Photoelectron Spectroscopy spectra taken at a photon energy of 12 keV on the as-grown sample (top curve) and for different levels of oxygen deficiency (increasing oxygen deficiency from top to bottom curves).

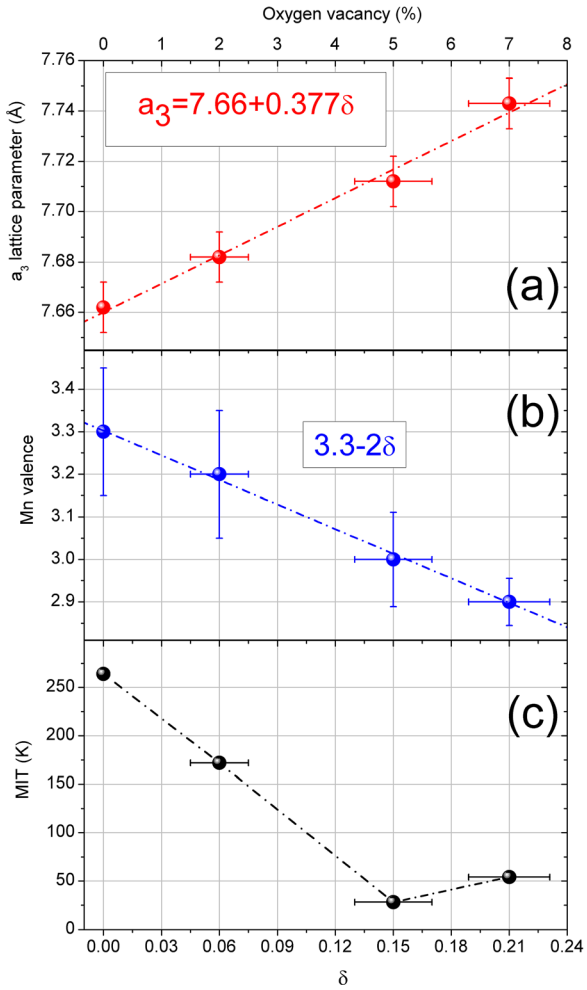

FIG. 4. Correlation between the (a) structural, (b) electronic, and (c) transport properties as a function of oxygen vacancies.

It can be seen that the HAXPES spectra for the La 3d remain unchanged independent on the amount of oxygen vacancies. Ca 2p HAXPES spectra have been also collected (not shown here) for each annealing process to control the La/Ca stoichiometry. We found that the initial stoichiometry is maintained independent on the oxygen deficiency. The Mn 3s core level peak also shows a doublet, which, for the case of manganese oxides, originates from the exchange coupling between the 3s hole and the 3d electrons together with a charge-transfer process. The magnitude of the splitting is indicative of the Mn formal valency.[15,16] The obtained energy splitting is 5.06 eV, 5.15 eV, 5.35 eV, and 5.45 eV, which corresponds to a formal Mn valency[15] of 3.3+, 3.2+, 3.0+, and 2.9+ for the as-grown sample, treatments a, b, and c, respectively. The oxygen vacancies δ can be calculated taking into account charge balance between the chemical elements forming the compound and their stoichiometry. In the $La_{0.7}Ca_{0.3}MnO_3$ compound, charge balance requires $\delta = (3.3\text{-Mn\_valence})/2$. δ parameter of 0, 0.05, 0.15, and 0.2 is obtained for the as-grown, treatment a, b, and c, respectively. It should be mentioned that such values are in perfect agreement with those obtained from the analysis of the O 1s HAXPES intensity. Based on the modification of the Mn 3s spectra and the unaltered La 3d spectra, it can be inferred that the oxygen vacancies are located at the octahedral basal plane.

A correlation between the electronic and atomic structure and the transport properties as a function of the oxygen vacancies can be hence established (Figure 4).

The sample is initially in a mixed Mn^{4+}/Mn^{3+} state, which transits to a lower Mn valence upon oxygen vacancies generation. The average Mn ionic radius increase induces an enlargement of the out-of-plane lattice parameter of the film. A linear increase is obtained as previously reported by Sun *et al.*,[17] although for thick films of lanthanum manganites doped with barium. The in-plane lattice parameters remain unchanged due to the epitaxial relation between the layer and the substrate. The location of the oxygen vacancies on the octahedral basal plane induces a gradual alignment of the Mn-O-Mn bond angle, which should enhance the charge transfer and hence increase the MIT. However, the MIT shifts linearly to lower temperatures with increasing the oxygen deficiency, except for the case of the perfect alignment of the MnO_6 blocks, as present for $\delta = 0.21$, for which the MIT shifts back to higher temperatures. The decrease of the transition temperature with oxygen deficiency, i.e., decrease of the Mn^{4+}/Mn^{3+} ratio, is in agreement with the dependence established by Cheong *et al.*[18] on $La_{1-x}Ca_xMnO_3$ compound. According to Cheong *et al.*, MIT is predicted to disappear for $Mn^{4+}/Mn^{3+} \sim 0.17$, in agreement with our experimental results. Hence, we can conclude that the transport properties on $La_{1-x}Ca_xMnO_3$ compound are mainly driven by the Mn valence state, although as demonstrated with a non-negligible contribution from the atomic structure, i.e., Mn-O-Mn bond angle and length.

Summarizing, using XRD, HAXPES, and transport techniques, we have established a correlation between the electronic, atomic and transport properties on $La_{0.7}Ca_{0.3}MnO_3$ thin films as a function of the oxygen vacancies. From the XRD and HAXPES spectra, we obtain that the oxygen vacancies are located exclusively in the basal plane of the MnO_6 block, which tend to align the Mn-O-Mn bond. The Mn valence is reduced with the consequent increase of the out-of-plane lattice parameter. A shift of the MIT to lower temperatures has been obtained, being the main responsible, the Mn valence modification and the lack of oxygen cation, which prevents the itinerant electron hopping.

The authors are grateful to the SpLine staff for their valuable help and to the financial support from the Spanish MINECO and Consejo Superior de Investigaciones Cientificas under Grant Nos. MAT2011-23785 and 20106OE013.

[1]A. de Andrés, J. Rubio, G. Castro, S. Taboada, J. L. Martínez, and J. M. Colino, Appl. Phys. Lett. **83**, 713 (2003).
[2]S. Jacob, T. Roch, F. S. Razavi, G. M. Gross, and H.-U. Habermeier, J. Appl. Phys. **91**, 2232 (2002).
[3]J. Z. Sun, D. W. Abraham, R. A. Rao, and C. B. Eom, Appl. Phys. Lett. **74**, 3017 (1999).
[4]J. Fontcuberta, B. Martínez, A. Seffar, S. Piñol, J. L. García-Muñoz, and X. Obradors, Phys. Rev. Lett. **76**, 1122 (1996).
[5]M. Jo, N. D. Mathur, N. K. Todd, and M. G. Blamire, Phys. Rev. B **61**, R14905 (2000).
[6]C. J. Lu, Z. L. Wang, C. Kwon, and Q. X. Jia, J. Appl. Phys. **88**, 4032 (2000).
[7]O. I. Lebedev, G. van Tendeloo, S. Amelinckx, B. Leibold, and H.-U. Habermeier, Phys. Rev. B **58**, 8065 (1998).

[8]M. Bibes, L. Balcells, S. Valencia, and J. Fontcuberta, Phys. Rev. Lett. **87**, 067210 (2001).
[9]T. Hahn, *International Tables for Crystallography* (Springer, Netherlands, 2006), Vol. A, p. 298.
[10]J. Rubio-Zuazo and G. R. Castro, Surf. Interface Anal. **40**, 1438 (2008).
[11]C. K. Jorgensen and H. Berthou, Chem. Phys. Lett. **13**, 186 (1972).
[12]H. Berthou and C. K. Jorgensen, Chem. Phys. Lett. **38**, 199 (1976).
[13]M. A. Brisk and A. D. Baker, J. Electron Spectrosc. Relat. Phenom. **7**, 197 (1975).
[14]W. Y. Howng and R. J. Thorn, Chem. Phys. Lett. **56**, 463 (1978).
[15]V. R. Galakhov, M. Demeter, S. Bartkowski, M. Neumann, N. A. Ovechkina, E. Z. Kurmaev, N. I. Lobachevskaya, Y. M. Mukovskii, J. Mitchell, and D. L. Ederer, Phys. Rev. B **65**, 113102 (2002).
[16]E. Beyreuther, S. Grafström, L. M. Eng, C. Thiele, and K. Dörr, Phys. Rev. B **73**, 155425 (2006).
[17]J. R. Sun, C. F. Yeung, K. Zhao, L. Z. Zhou, C. H. Leung, H. K. Wong, and B. G. Shen, Appl. Phys. Lett. **76**, 1164 (2000).
[18]P. Schiffer, A. P. Ramirez, W. Bao, and S.-W. Cheong, Phys. Rev. Lett. **75**, 3336 (1995).